

# Graphene Rings in Magnetic Fields: Aharonov-Bohm Effect and Valley Splitting

J Wurm<sup>1,2</sup>, M Wimmer<sup>1</sup>, H U Baranger<sup>2</sup> and K Richter<sup>1</sup>

<sup>1</sup>Institut für Theoretische Physik, Universität Regensburg, D-93040, Germany

<sup>2</sup>Department of Physics, Duke University, Box 90305, Durham, North Carolina 27708-0305, U.S.A.

E-mail: Juergen.Wurm@physik.uni-regensburg.de

**Abstract.** We study the conductance of mesoscopic graphene rings in the presence of a perpendicular magnetic field by means of numerical calculations based on a tight-binding model. First, we consider the magnetoconductance of such rings and observe the Aharonov-Bohm effect. We investigate different regimes of the magnetic flux up to the quantum Hall regime, where the Aharonov-Bohm oscillations are suppressed. Results for both clean (ballistic) and disordered (diffusive) rings are presented. Second, we study rings with smooth mass boundary that are weakly coupled to leads. We show that the valley degeneracy of the eigenstates in closed graphene rings can be lifted by a small magnetic flux, and that this lifting can be observed in the transport properties of the system.

## 1. Introduction

Since their experimental discovery, graphite monolayers, also known as graphene, have attracted a huge amount of interest among both experimentalists and theorists due to the linear low energy dispersion and various properties stemming from this unusual dispersion [1, 2]. For instance, graphene has opened new perspectives for mesoscopic physics, such as pseudodiffusive conductance at the Dirac point [3, 4, 5], specular Andreev reflection [6], or the signatures of symmetries of the graphene Hamiltonian in the conductance of diffusive wires [7, 8, 9, 10, 11] and ballistic cavities [12, 13].

Mesoscopic rings can be considered as prototypical devices in mesoscopic physics, as they show one of the most basic coherence effects, namely the Aharonov-Bohm (AB) effect [14, 15, 16]: oscillations of the transmission, or dimensionless conductance,  $T = (h/2e^2)G$  as a function of the magnetic flux  $\Phi$  through the ring. The reason for these oscillations is the phase difference  $\Delta\varphi = 2\pi\Phi/\Phi_0$  between electrons travelling along the different arms of the ring. Here,  $\Phi_0 = h/e$  is the magnetic flux quantum. Fifty years after its discovery, the AB effect is one of the most well-known manifestations of quantum interference within and beyond the field of condensed matter physics.

Hence it is rather surprising that the AB effect in graphene has up to now received only a little attention in the literature. Most notably, there are only two experiments

on graphene AB rings manufactured by electron beam lithography [17, 18], one of them leaving many open questions on the physical origin of some of the observed effects [17]. From the theory side, there is only one numerical study of the AB effect in graphene rings; it focuses on the effects of valley-polarized currents, i.e. on the few-mode or low-doping regime in the leads [19]. In this work, we will in contrast also consider the many-mode or high-doping regime.

In addition to these studies focusing on the transport properties of *open* rings, there has been a proposal to use the Aharonov-Bohm effect in *closed* rings to form qubits: The energy spectrum of a closed graphene ring with infinite mass boundary condition [20] has been calculated in reference [21], where the authors find that the valley degeneracy of the energy levels is lifted as soon as a magnetic flux pierces the ring. This effect has also been found for chaotic graphene quantum dots [13]. Note that this aspect is not present in AB rings realized e.g. in semiconductor heterostructures and metals. It is connected to a special antiunitary symmetry of the Dirac Hamiltonian, which describes graphene well for low Fermi energies. In this work, we will show that the lifting of the valley degeneracy is also visible in the transport properties of graphene rings.

The paper is organized as follows: In the first part, we investigate the AB effect of graphene structures by numerically calculating the transmission of rings attached to infinitely extended leads. We study both small rings in the one-mode regime and large rings with many modes propagating in both the leads and arms of the ring. In the latter we especially consider the high-field regime and the effects of disorder. In the second part of this work, we show that the breaking of valley-degeneracy by a magnetic field is also visible in the transport properties of graphene rings. We do this by numerically calculating the transmission of graphene rings that are weakly coupled to two leads. This transmission shows peaks as a function of the Fermi energy  $E_F$  which correspond to the energy levels of a closed ring; the lifting of their degeneracy can be observed as a splitting of the transmission peaks upon applying a magnetic field perpendicular to the ring.

For our numerical work, we use a tight binding model taking into account the  $2p_z$ -orbitals of the carbon atoms, leading to the Hamiltonian

$$H_{\text{tb}} = \sum_{\langle i,j \rangle} t_{ij} c_i^\dagger c_j + \sum_i m_i c_i^\dagger c_i \quad (1)$$

with  $i$  and  $j$  being nearest neighbor sites in the first sum. The magnetic field is included via the Peierls substitution  $t_{ij} = -t \exp\left(i \frac{2\pi}{\Phi_0} \int_{\mathbf{r}_i}^{\mathbf{r}_j} \mathbf{A} \cdot d\mathbf{r}\right)$ . The second term accounts for a staggered on-site potential, i. e.  $m_i = m(\mathbf{r}_i)$  is positive (negative) if  $\mathbf{r}_i$  is located on sublattice A (B). Such a staggered potential corresponds to a mass term in the effective Dirac equation and will be used in the second part of this paper to suppress the inter-valley scattering that breaks the valley degeneracy [13]. The lattice points are determined by cutting a ring out of the graphene sheet [cf. figure 1 (b)]. In order to solve the transport problem to obtain the dimensionless conductance  $T$  within this tight-binding model, we use an adaptive recursive Green function method [22].

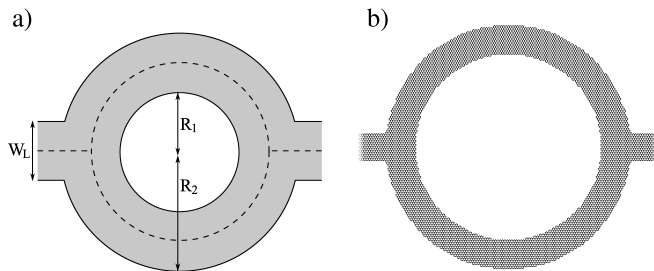


**Figure 1.** (a) Schematic of the systems studied numerically. The parameters defining the shape are the inner and outer radius  $R_1$  and  $R_2$ , respectively, and the width  $W_L$  of the infinitely extended leads. The dashed line marks the points where the mass term used in Section 3 is zero. (b) Example of a system defined by cutting a ring out of a graphene sheet [the system was used for figure 2 (a) and (c)].

## 2. Aharonov-Bohm effect in graphene rings

We now investigate the transmission of graphene rings with two attached leads under the influence of a perpendicular magnetic field  $B$ , giving rise to a flux  $\Phi$  through the ring. In the following we define  $\Phi = B \pi \bar{R}^2$  as the flux through a circle with the average ring radius  $\bar{R} = (R_1 + R_2)/2$  (cf. figure 1). Because electrons can travel along one or the other arm of the ring, the transmission  $T(\Phi)$  is expected to oscillate with periods  $\Delta\Phi = \Phi_0/n$ ,  $n \in \mathbb{N}$ , as mentioned in the introduction. The reason why more than one single period, namely  $\Phi_0$ , may occur is that the electrons do not necessarily have to leave the ring after traversing an arm once, but rather they may circle around the ring several times before exiting, giving rise to higher harmonics with  $n > 1$ .

We begin by considering small graphene rings in the one-mode regime. In figure 2(a) and (b) we show the numerically calculated transmission as a function of  $\Phi$  for two small rings with radii of about 10 nm and widths of about 3 nm (see figure caption for details). One of the rings has zigzag type leads while the other has armchair type leads. For both, one can clearly see the AB oscillations with period  $\Phi = \Phi_0$ . To expose a few more details of the frequency content of our data, we show the power spectra of the AB oscillations in figure 2(c) and (d). There we find pronounced peaks for the fundamental frequency and for several higher harmonics (we show only the first five). Note that we plot the spectra on a logarithmic scale, since the fundamental frequency is strongly dominating over the higher ones. The peaks in the spectrum lie very close to multiple values of  $1/\Phi_0$ . Because of the finite width of the rings, one has certain allowed deviations from these values. For example, for the system of figure 2(a), the fundamental frequency is expected to lie between  $0.74/\Phi_0$  and  $1.3/\Phi_0$ , obtained from the inner and outer ring radii  $R_1$  and  $R_2$ , respectively. The fact that the peaks are slightly shifted to frequencies lower than  $n/\Phi_0$  means that the effective radius of our rings is slightly smaller than the average radius  $\bar{R}$ . We also performed calculations for various systems with different parameters and found the same behavior irrespective of the details like radii, width or lead type.

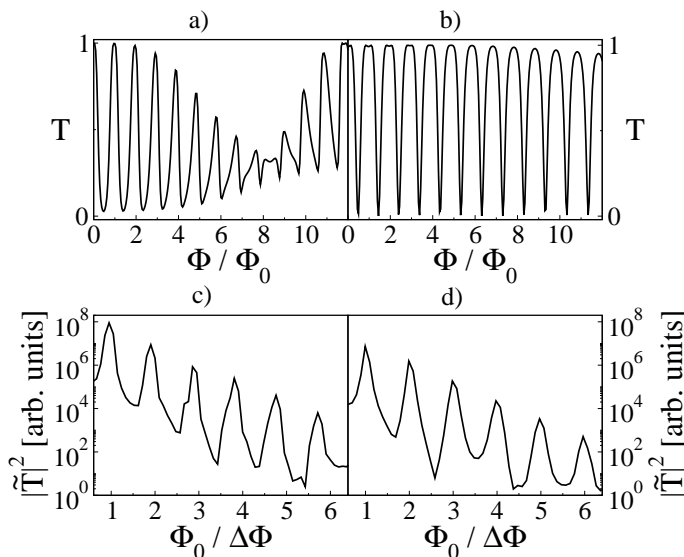


**Figure 2.** Aharonov-Bohm oscillations [(a),(b)] and corresponding power spectra [(c),(d)] of small rings in the one-mode regime. (a),(c) Ring with zigzag type leads and  $R_1 = 9.84$  nm,  $R_2 = 13.0$  nm,  $W_L = 3.20$  nm. (b), (d) Ring with armchair type leads and  $R_1 = 9.84$  nm,  $R_2 = 12.5$  nm,  $W_L = 4.92$  nm.  $\bar{T}(1/\Delta\Phi)$  is the Fourier transform of  $T(\Phi)$  where  $\Delta\Phi$  is the period of the oscillation related to the Fourier transform variable by  $k = 2\pi/\Delta\Phi$ .

Next, we turn to the case of larger graphene rings in the many-mode regime, i.e. for high values of doping. This is the regime applicable to the available experiments of Refs. [17, 18]. In the numerical simulations we consider rings with an average radius  $\bar{R} \approx 55$  nm. While this size is still smaller than in the experiments ( $\bar{R} \approx 500$  nm in Ref. [17] and  $\bar{R} \approx 250$ -300 nm in Ref. [18]), the rings contain more than a hundred thousand atoms and hence can be considered as mesoscopic objects. Therefore, we do not expect that larger rings would show any fundamentally different physical properties than the systems considered here.

In figure 3, we show the magnetoconductance of a large ring for a wide range of the magnetic flux, up to the quantum Hall regime. Up to a flux of about  $300 \Phi_0$ , we see AB oscillations with amplitudes approximately in the range  $\Delta T \approx 0.5 - 1$  [see also figure 5(a)]. For fluxes larger than  $300 \Phi_0$ , the oscillation amplitude becomes significantly smaller ( $\Delta T \lesssim 0.5$ ), while for even higher values of  $\Phi$  the oscillations vanish completely and the transmission is equal to the maximum value given by the number of quantum Hall edge channels in the leads. This behavior can be understood by the following picture. The cyclotron diameter  $d_c$  in (bulk) graphene is given by

$$d_c = \frac{2E_F}{v_F e B}, \quad (2)$$

where  $E_F$  is the Fermi energy and  $v_F$  is the Fermi velocity. In our case  $E_F = 0.3t$  and the width of the ring arms is  $W_A \approx 18$  nm. This means, that at a flux of  $\Phi \approx 230 \Phi_0$ , the cyclotron diameter is equal to an arm's width. When  $\Phi$  becomes comparable to this value, it becomes more probable that the electron enters one arm than the other, because

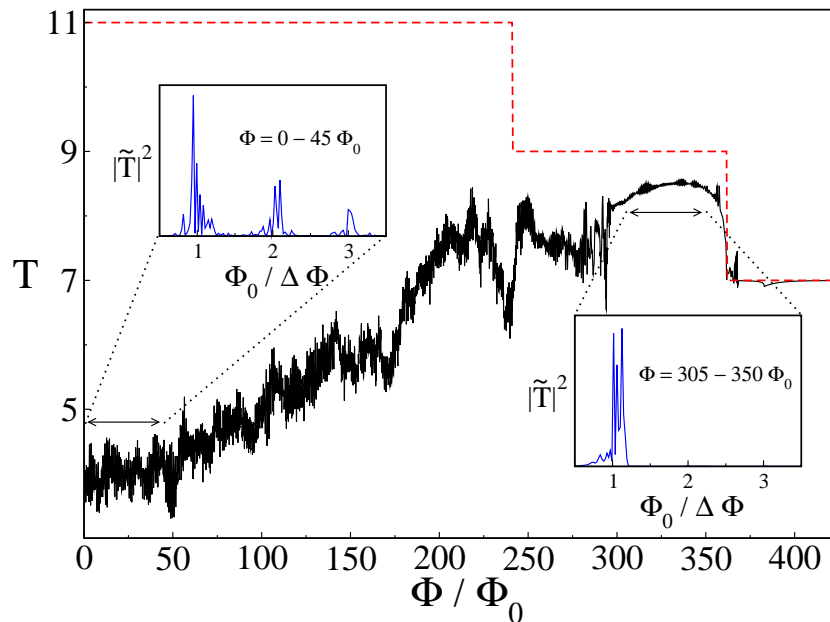


**Figure 3.** Magnetotransmission of a large ring with  $R_1 = 45.5$  nm,  $R_2 = 63.7$  nm and  $W_L = 13.5$  nm for a wide range of the magnetic flux  $\Phi$  (solid black line) in the multi-mode regime. The red dashed line shows the number of occupied transverse channels in the leads. The insets show power spectra for different regimes: left inset  $\Phi = 0-45 \Phi_0$ , right inset  $\Phi = 305-350 \Phi_0$ .

the magnetic field dictates the direction of classical propagation. Therefore, interference is reduced. When the magnetic field gets larger and larger, it becomes more and more unlikely for the electron to enter the second arm, and finally the interference vanishes when the quantum Hall edge channels fully form. Since backscattering is also strongly reduced at large magnetic fields, the transmission is only limited by the number of propagating lead channels. This number however is reduced for a fixed Fermi energy as the magnetic field is increased (the distance between the Landau levels increases with  $B$ ), which leads to the step-like transmission in this regime. Furthermore, classical cyclotron effects are also important at the entrance to the ring. At low fields, a large part of the wavefunction entering the ring is simply reflected back into the lead by the inner wall of the ring. As the field gets higher, the probability to turn around the corner into one of the arms increases.

This scenario is shown in figure 4: the absolute value of the current density in the ring is given for values of the flux  $\Phi$  corresponding to the different regimes. For  $\Phi = 113 \Phi_0$  [figure 4(a)] – the low transmission regime – the current flows more or less equally through both arms. As the flux is increased, the electrons are forced more and more into the upper arm, and at very high fluxes, when electrons are essentially travelling only along the upper arm, interference gets suppressed and finally vanishes. Note that also the quantum Hall edge channels become clearly visible at high fluxes. It is worth noting that the small AB oscillations in the regime where  $\Phi \gtrsim 300 \Phi_0$  are not due to electrons entering the lower arm of the ring from the left lead. If this were true,

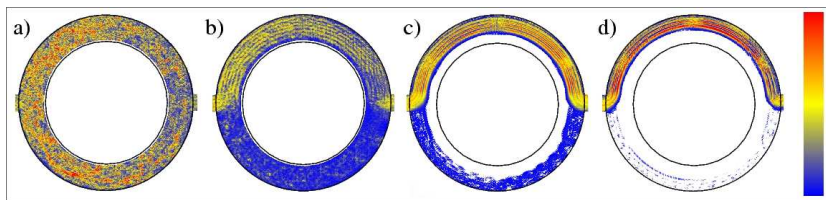


**Figure 4.** Absolute value of the current density in the ring of figure 3. The electrons enter the ring from the left lead. Blue means low and red means high current density. (a)  $\Phi = 113 \Phi_0$  (b)  $\Phi = 204 \Phi_0$  (c)  $\Phi = 328 \Phi_0$  (d)  $\Phi = 453 \Phi_0$ .

the current in figure 4 (c) would be localized at the inner border of the lower arm, which is obviously not the case. In this regime, the interference is due to paths going along the upper arm and leaving the ring after a half circle interfering with paths which also start along the upper arm but which go around the ring one more time before exiting. Such paths also give rise to oscillations with period  $\Phi_0$ . Note that this effect is present only because the lead width in the chosen geometry is somewhat smaller than the width of the ring, as then the quantum Hall edge channels in the ring arms may be scattered at the lead opening and enter the opposite arm. Hence, this regime corresponds to interferometry with quantum Hall edge channels. When the lead width is larger than the ring arm width, scattering at the lead openings is suppressed, and no interference is observed. The power spectra shown as insets in figure 3 also support this picture: For low fields, several higher harmonics are present, whereas at high fields only the fundamental frequency is visible because multiple windings around the ring are strongly suppressed in the quantum Hall regime.

The magnitude of the conductance seen in the quantum Hall regime – an odd integer times  $2e^2/h$  (see figure 3) – is consistent with the bulk quantum Hall effect [23, 24] as well as with theoretical results obtained for graphene nanoribbons [25]. (Recall that in a two terminal geometry the conductance shows the quantization of  $\sigma_{xy}$ .) The steps of magnitude 2 are easily understood in terms of the valley degeneracy of the subbands in the leads. The quantization at odd rather than even integers is explained by a Berry phase effect involving the pseudospin associated with the sub-lattice degree of freedom [2].

In the experimental work of Ref. [17], a significant increase of the AB oscillation amplitude was observed at high fields when  $W_A \gtrsim d_c$ . Note that our data in figure 3 does not show any such increase (if anything, it shows the opposite). To investigate this further, figure 5 shows the oscillating part of the magnetoconductance for a range of  $\Phi$  near the value where the cyclotron diameter becomes equal to the width of a ring arm [around  $230 \Phi_0$  according to (2)]. The authors of [17] speculate that an asymmetry between the two ring arms could be responsible for the increase of the oscillation amplitude. Our numerical calculations, however, do not confirm this: for figure 5 (b) we reduced the width of one arm by 10 percent, but also in this case, an increase of the oscillation amplitude at high magnetic fields is absent.

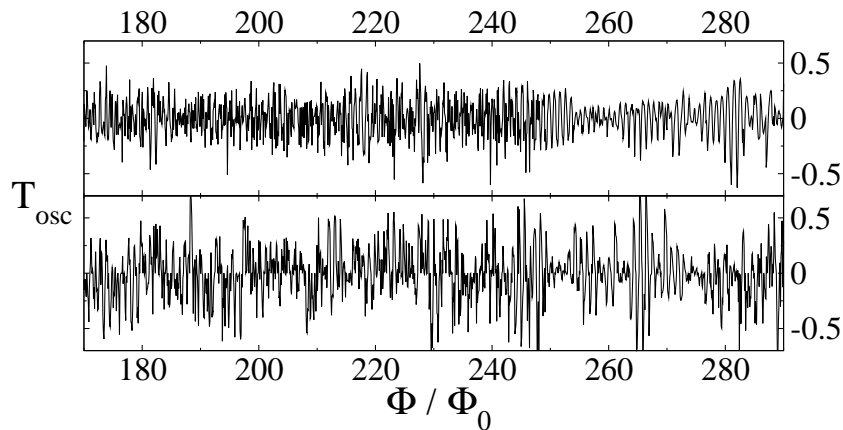


**Figure 5.** Oscillating part of the magnetotransmission. The average transmission of one period around the corresponding value of  $\Phi$  has been subtracted from  $T(\Phi)$  to obtain  $T_{\text{osc}}(\Phi)$ . Top panel: System of figure 3. Lower panel: Same system as in the top panel, but the outer radius of one ring arm is reduced from 63.7 nm to 61.9 nm which results in a difference in the arm widths of 10 percent.

The formation of quantum Hall edge channels in a clean system happens for  $d_c \approx W_A$ , as observed in our simulations (figure 3). In the data of Ref. [17], however, AB oscillations are still visible even for much higher magnetic fields, when  $d_c < W_A$ . Furthermore, despite being ten times larger than the rings considered in our numerical studies, the average conductance in the highly doped regime is only on the order of a few  $\frac{e^2}{h}$ . These two features are a strong indication that these experiments are in the strongly disordered regime.

Hence, we now turn to briefly discussing the effects of disorder on the AB oscillations. For this, we consider both edge disorder (employing the model of edge disorder from Ref. [26]) and bulk disorder (using Gaussian disorder as in Ref. [28]). Figure 6(a) and (b) show the magnetoconductance for edge and bulk disorder, respectively. In the case of edge disorder only, we still observe an increase of the transmission with magnetic field due to classical cyclotron effects as in the clean case. In addition, the onset of quantized Hall conductance is only shifted slightly to higher fields. In fact, since the interior of the ring arms is ballistic, we still expect quantum Hall edge channels to form for  $d_c \approx W_A$ . Moreover, as in the clean case we observe interference of quantum Hall edge states for  $\Phi \gtrsim 300 \Phi_0$ . In contrast, for bulk disorder the transmission probability remains – apart from conductance fluctuations – virtually unchanged as the magnetic field increases. In this case, the disorder broadens the Landau levels enough to prevent the formation of edge channels. The similarity of this behavior to that of the experiments reported in Ref. [17] suggests that the experiments are in the “dirty limit”, dominated by bulk disorder. Such a conclusion is also in agreement with Ref. [18] where their experimental results for AB rings are explained in terms of diffusive metallic transport.

Further characteristics of the diffusive limit include that the system remains isotropic for higher fields, both ring arms carry an equal amount of current, and higher

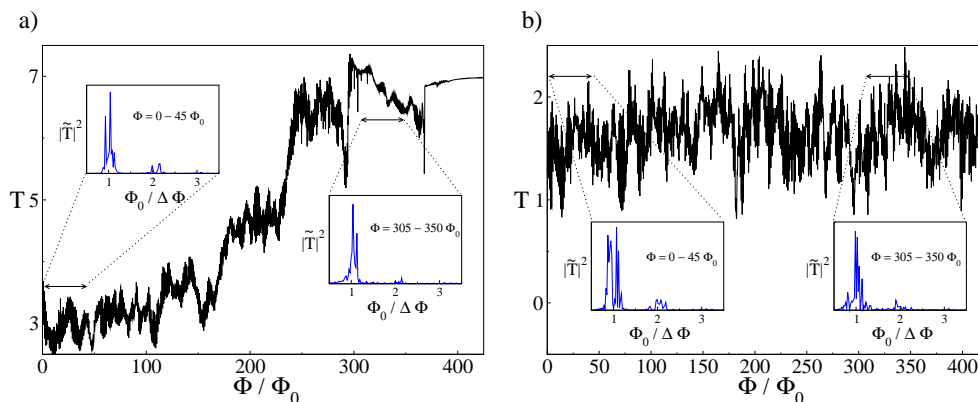


**Figure 6.** Magnetotransmission of disordered rings with  $R_1 = 45.5 \text{ nm}$ ,  $R_2 = 63.7 \text{ nm}$  and  $W_L = 13.5 \text{ nm}$  in the multi-mode regime (solid black lines). The insets show corresponding power spectra. (a) Ring with edge disorder. Here, we employed the etching disorder model of Ref. [26] with  $N_{\text{sweeps}} = 30$  and  $p_i = 0.05$  for  $i = 1 \dots 30$  (for the details on the parameters of this model, see Ref. [26]). (b) Ring with bulk disorder. For the bulk disorder, we choose a Gaussian disorder potential with  $N_{\text{imp}}/N_{\text{tot}} = 0.05$ ,  $\delta = 0.1t$  and  $\xi = 2a$  (for the details on the parameters of this model, see Ref. [27]). Note that although the Gaussian disorder potential is smooth on the lattice scale and hence does not scatter the valleys, valley scattering nevertheless happens at the abrupt termination of the lattice at the edges.

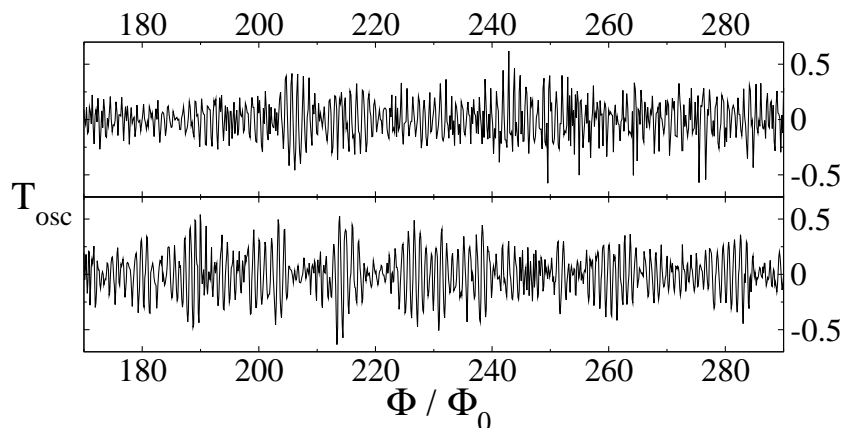


**Figure 7.** Oscillating part of the magnetotransmission for disordered rings. Top panel: System with edge disorder. Lower panel: System with Gaussian bulk disorder. Disorder parameters are as in figure 6.

harmonics are suppressed in comparison to the clean case (see figure 3). Finally, figure 7 shows the oscillating part of the magnetoconductance in the vicinity of  $d_c \approx W_A$ . Again, the size of the oscillations remains essentially unchanged with increasing magnetic flux.

A closer inspection of the oscillations reveals that in the case of edge disorder, there are also aperiodic oscillations on top of the periodic AB oscillations for  $\Phi \approx 250 - 300 \Phi_0$ , where we observe the onset of edge channel formation. These aperiodic oscillations are presumably due to localization and resonant tunneling at the disordered edge,



since there is still backscattering among the not fully formed edge states. This interpretation is supported by the fact that the aperiodic oscillations are absent in the case of bulk disorder, where the edge channel formation is completely suppressed. Furthermore, note that aperiodic oscillations are also present (although to a less degree) for  $\Phi \approx 190 - 250 \Phi_0$  in the clean rings, as the abrupt lattice termination also serves as a source of *local* disorder.

### 3. Breaking the valley degeneracy in graphene rings

In the following, we demonstrate numerically that the lifting of the valley degeneracy of eigenstates in rings by a magnetic field perpendicular to the ring is also visible in transport properties of the ring. In Ref. [21], the authors calculate the energy spectrum of a closed graphene ring with infinite mass boundary condition [20] within the effective Dirac theory. The energy levels  $E_{\tau\pm}^{nm}$  are labeled by a radial quantum number  $n$ , an angular momentum quantum number  $m$ , valley index  $\tau$  and the sign of the energy. At zero magnetic field, the authors find from their calculation the degeneracy  $E_{-\tau\pm}^{n(-m)} = E_{\tau\pm}^{nm}$ , which is not present when a perpendicular magnetic field is applied. It is worth to point out that this is due to the fact that in addition to the usual time reversal (TR) operator  $\mathcal{T} = (\sigma_y \otimes \tau_y)\mathcal{C}$ , there is another antiunitary operator commuting with the Hamiltonian at zero magnetic field, namely  $\mathcal{T}_v = (\sigma_y \otimes \tau_x)\mathcal{C}$ . In contrast to  $\mathcal{T}$ ,  $\mathcal{T}_v$  is associated with a symplectic symmetry, since  $\mathcal{T}_v^2 = -1$ . This ensures the degeneracy of both valleys (Kramer's degeneracy [29]). Note that this reasoning holds only if the boundary condition preserves the symmetry connected with  $\mathcal{T}_v$ ; such is the case for the infinite mass boundary condition used in Ref. [21] but is not the case, for example, for valley mixing armchair boundaries. Once a magnetic field pierces the ring, the  $\mathcal{T}_v$  symmetry is broken and the valley degeneracy is lifted. This mechanism has been numerically observed in ballistic graphene quantum dots with smooth mass confinement [13], where the amplitude of universal conductance fluctuations was considered. Here we follow a different idea to probe the effect of breaking valley degeneracy with a magnetic field, namely we calculate numerically the conductance of a ring weakly coupled to two leads. The conductance is then expected to be peaked at values of the Fermi energy that match the energies of eigenstates of the closed ring.

In order to have valley degenerate states at zero magnetic field, we have to avoid scattering at local armchair boundaries, as mentioned above. To model the infinite mass boundary numerically, we use smooth mass confinement as introduced in [13]. Due to the finite escape time of electrons injected into the ring from one lead, the effects of inter-valley scattering will be suppressed in such a system, provided the mass confinement is smooth enough. We use a mass term that is zero in the middle of the ring and increases quadratically towards the boundaries [cf. figure 1 (a)]:  $m(x, y) = \omega^2 \delta^2(x, y)/2$ , where  $\delta(x, y) = \sqrt{x^2 + y^2} - \bar{R}$  for a ring with average radius  $\bar{R}$  centered at  $x = y = 0$ . In the leads we use a consistent mass term, with  $\delta(x, y) = y$  for leads in the  $x$ -direction. In the region where the leads are attached, we match both terms in a smooth way. In this

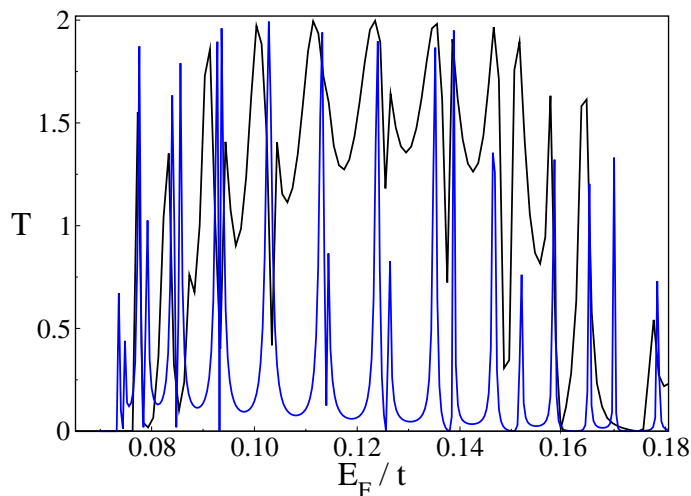


**Figure 8.** Transmission of rings with smooth mass term ( $\omega = 0.05\sqrt{t}/a$ ) and  $R_1 = 9.84\text{nm}$ ,  $R_2 = 19.7\text{nm}$ ,  $W_L = 9.84\text{nm}$ , with leads that are strongly (black) and weakly (blue) coupled to the system as a function of the Fermi energy in the two-mode regime (transverse lead channels are twofold valley degenerate).

region we also introduce a mass-induced barrier, that can be varied in height, in order to tune the coupling strength between leads and ring.

Figure 8 shows the transmission of rings with both strong and weak coupling as a function of the Fermi energy  $E_F$ . We checked that the transmission is insensitive to the orientation of the system with respect to the lattice orientation at the energies considered. This means that the detailed edge structure of ring and leads do not play a role, and implies that the mass confinement is smooth enough to suppress inter-valley scattering. Upon reducing the coupling strength, the oscillations in the transmission of the ring with strongly coupled leads turn into sharp peaks. The system studied is a ring with  $R_1 = 9.84\text{nm}$ ,  $R_2 = 19.7\text{nm}$  and width  $W_L = 9.84\text{nm}$ . Note that the effective width of leads and ring is reduced due to the mass confinement. The mass potential is  $0.5t$  at the physical borders of the system for the value of  $\omega$  used (see caption of figure 8).

To find out, whether the energy spectrum of our ring shows the valley degeneracy connected with the symmetry described by  $\mathcal{T}_v$ , we try to break this supposed degeneracy by applying a magnetic field perpendicular to the ring. Figure 9 (a) shows the numerical results, where the magnetic flux through the area  $\pi\bar{R}^2$  with  $\bar{R} = 14.8\text{nm}$  is  $\Phi = 0$  (dashed lines) and  $\Phi = 0.17\Phi_0$  (solid lines), respectively. We find that the transmission peaks split and that their heights are in general reduced. This is the behavior expected from degeneracy lifting, as the weight of each split peak now corresponds to only a single, non-degenerate level. Note that for  $E < 0.14t$  the peaks partially overlap; the splitting of the valley degeneracy is particularly clear for  $E > 0.14t$  where the peaks are well separated, as shown in figure 9 (b). These results show unambiguously that the lifting of the valley-degeneracy by a magnetic flux in weakly coupled graphene rings can also be observed in the transport properties.

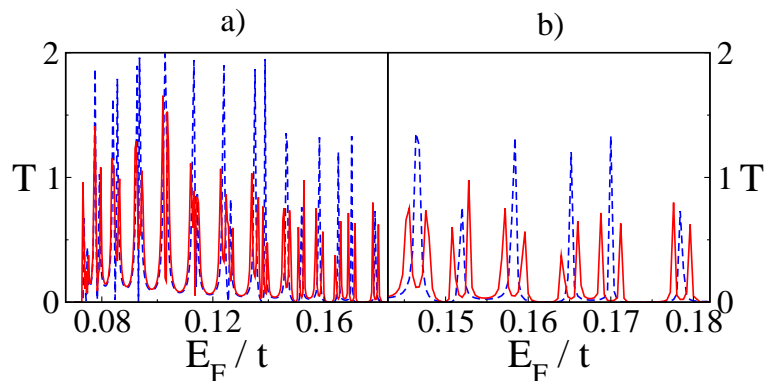


**Figure 9.** Transmission of the weakly coupled ring from figure 8 for zero flux (blue dashed lines) and a flux  $\Phi = 0.17 \Phi_0$  (red solid lines). (b) shows a zoom on the 6 (or 12, respectively) rightmost peaks of (a).

#### 4. Conclusion

In this work we have investigated two different aspects of mesoscopic graphene rings: First, we have numerically studied the Aharonov-Bohm effect in rings cut out of the graphene lattice. Both small rings with a single mode as well as large rings supporting many modes exhibit clear  $h/e$  Aharonov-Bohm oscillations. Although disorder has a strong influence on the average transmission of graphene rings especially in the high field regime, the Aharonov-Bohm oscillations are influenced only very little by both edge and bulk disorder. Second, we have shown that the signature of the splitting of the valley-degeneracy by a magnetic field in rings with a mass confinement can also be observed in the transport properties of rings that are weakly coupled to leads.

#### Acknowledgments

JW acknowledges support from Deutsche Forschungsgemeinschaft within GRK 638, and MW and KR support from Deutsche Forschungsgemeinschaft within SFB 689. The work at Duke was supported in part by the U.S. NSF (DMR-0506953) and the DAAD. We would like to thank İnanç Adagideli, Patrik Recher, Adam Rycerz and Björn Trauzettel for helpful discussions.

- [1] A. K. Geim and K. S. Novoselov. The rise of graphene. *Nature Mat.*, 6(3):183–191, March 2007.
- [2] A. H. Castro Neto, F. Guinea, N. M. R. Peres, K. S. Novoselov, and A. K. Geim. The electronic properties of graphene. *Rev. Mod. Phys.*, 81(1):109, 2009.
- [3] J. Tworzydło, B. Trauzettel, M. Titov, A. Rycerz, and C. W. J. Beenakker. Sub-Poissonian shot noise in graphene. *Phys. Rev. Lett.*, 96(24):246802, 2006.
- [4] R. Danneau, F. Wu, M. F. Craciun, S. Russo, M. Y. Tomi, J. Salmilehto, A. F. Morpurgo, and P. J. Hakonen. Shot noise in ballistic graphene. *Phys. Rev. Lett.*, 100(19):196802, 2008.
- [5] L. DiCarlo, J. R. Williams, Yiming Zhang, D. T. McClure, and C. M. Marcus. Shot noise in graphene. *Phys. Rev. Lett.*, 100(15):156801, 2008.
- [6] C. W. J. Beenakker. Colloquium: Andreev reflection and Klein tunneling in graphene. *Rev. Mod. Phys.*, 80(4):1337, 2008.

- [7] H. Suzuura and T. Ando. Crossover from symplectic to orthogonal class in a two-dimensional honeycomb lattice. *Phys. Rev. Lett.*, 89(26):266603, Dec 2002.
- [8] D. V. Khvashchenko. Electron localization properties in graphene. *Phys. Rev. Lett.*, 97(3):036802, 2006.
- [9] E. McCann, K. Kechedzhi, Vladimir I. Fal'ko, H. Suzuura, T. Ando, and B. L. Altshuler. Weak-localization magnetoresistance and valley symmetry in graphene. *Phys. Rev. Lett.*, 97(14):146805, 2006.
- [10] A. F. Morpurgo and F. Guinea. Intervalley scattering, long-range disorder, and effective time-reversal symmetry breaking in graphene. *Phys. Rev. Lett.*, 97(19):196804, 2006.
- [11] I. L. Aleiner and K. B. Efetov. Effect of disorder on transport in graphene. *Phys. Rev. Lett.*, 97(23):236801, 2006.
- [12] L. A. Ponomarenko, F. Schedin, M. I. Katsnelson, R. Yang, E. W. Hill, K. S. Novoselov, and A. K. Geim. Chaotic Dirac billiard in graphene quantum dots. *Science*, 320(5874):356–358, 2008.
- [13] J. Wurm, A. Rycerz, I. Adagideli, M. Wimmer, K. Richter, and H. U. Baranger. Symmetry classes in graphene quantum dots: Universal spectral statistics, weak localization, and conductance fluctuations. *Phys. Rev. Lett.*, 102(5):056806, 2009.
- [14] Y. Aharonov and D. Bohm. Significance of electromagnetic potentials in the quantum theory. *Phys. Rev.*, 115(3):485–491, Aug 1959.
- [15] R. A. Webb, S. Washburn, C. P. Umbach, and R. B. Laibowitz. Observation of  $h/e$  Aharonov-Bohm oscillations in normal-metal rings. *Phys. Rev. Lett.*, 54(25):2696–2699, Jun 1985.
- [16] S. Washburn and R. A. Webb. Aharonov-Bohm effect in normal metal quantum coherence and transport. *Adv. Phys.*, 35(4):375–422, 1986.
- [17] S. Russo, J. B. Oostinga, D. Wehenkel, H. B. Heersche, S. S. Sobhani, L. M. K. Vandersypen, and A. F. Morpurgo. Observation of Aharonov-Bohm conductance oscillations in a graphene ring. *Phys. Rev. B*, 77(8):085413, 2008.
- [18] F. Molitor, M. Huefner, A. Jacobsen, A. Pioda, C. Stampfer, K. Ensslin, and T. Ihn. Aharonov-Bohm effect in a side-gated graphene ring. arXiv:0904.1364v1, 2009.
- [19] A. Rycerz. Aharonov-Bohm effect and valley polarization in nanoscopic graphene rings. *Acta Phys. Pol. A*, 115(1):322–325, 2009.
- [20] M. V. Berry and R. J. Mondragon. Neutrino billiards: Time-reversal symmetry-breaking without magnetic fields. *Proc. R. Soc. Lond. A*, 412:53–74, 1987.
- [21] P. Recher, B. Trauzettel, A. Rycerz, Ya. M. Blanter, C. W. J. Beenakker, and A. F. Morpurgo. Aharonov-Bohm effect and broken valley degeneracy in graphene rings. *Phys. Rev. B*, 76(23):235404, 2007.
- [22] M. Wimmer and K. Richter. Optimal block-tridiagonalization of matrices for coherent charge transport. arXiv:0806.2739v1, 2008.
- [23] K. S. Novoselov, A. K. Geim, S. V. Morozov, D. Jiang, M. I. Katsnelson, I. V. Grigorieva, S. V. Dubonos, and A. A. Firsov. Two-dimensional gas of massless Dirac fermions in graphene. *Nature*, 438(7065):197–200, November 2005.
- [24] Y. Zhang, Y.-W. Tan, H. L. Stormer, and P. Kim. Experimental observation of the quantum Hall effect and Berry's phase in graphene. *Nature*, 438(7065):201–204, 2005.
- [25] L. Brey and H. A. Fertig. Edge states and the quantized Hall effect in graphene. *Phys. Rev. B*, 73(19):195408, 2006.
- [26] E. R. Mucciolo, A. H. Castro Neto, and C. H. Lewenkopf. Conductance quantization and transport gaps in disordered graphene nanoribbons. *Phys. Rev. B*, 79(7):075407, 2009.
- [27] A. Rycerz, J. Tworzydło, and C. W. J. Beenakker. Valley filter and valley valve in graphene. *Nature Phys.*, 3(3):172–175, March 2007.
- [28] A. Rycerz, J. Tworzydło, and C. W. J. Beenakker. Anomalously large conductance fluctuations in weakly disordered graphene. *Europhys. Lett.*, 79(5):57003, 2007.
- [29] A. Messiah. *Quantum Mechanics 2*. North-Holland, 1970.